



Colorimetric and Raman dual-mode lateral flow immunoassay detection of SARS-CoV-2 N protein antibody based on Ag nanoparticles with ultrathin Au shell assembled onto Fe₃O₄ nanoparticles

Jingwen Li¹ · Penghui Liang¹ · Tianyu Zhao¹ · Gengchen Guo¹ · Jinyue Zhu¹ · Congying Wen¹ · Jingbin Zeng¹

Received: 23 August 2022 / Revised: 27 October 2022 / Accepted: 14 November 2022 / Published online: 22 November 2022
© Springer-Verlag GmbH Germany, part of Springer Nature 2022

Abstract

Serological antibody tests are useful complements of nuclei acid detection for SARS-CoV-2 diagnosis, which can significantly improve diagnostic accuracy. However, antibody detection in serum or plasma remains challenging to do with high sensitivity. In this study, Ag nanoparticles with ultra-thin Au shells embedded with 4-mercaptobenzoic acid (MBA) (Ag^{MBA}@Au) were manufactured and then assembled onto Fe₃O₄ surface by electrostatic interaction to construct the Fe₃O₄-Ag^{MBA}@Au nanoparticles (NPs) with magnetic-Raman-colorimetric properties. Based on the composite nanoparticles, a colorimetric and Raman dual-mode lateral flow immunoassay (LFIA) for ultrasensitive identification of SARS-CoV-2 nucleocapsid (N) protein antibody was constructed. The magnetic nanoparticles (Fe₃O₄ NPs) were acted as the core and coated a layer of Ag^{MBA}@Au particles on the surface by electrostatic interaction to prepare Fe₃O₄-Ag^{MBA}@Au NPs, which can amplify the SERS signal due to multiple Ag^{MBA}@Au particles concentrated on a single magnetic nanoparticle. Moreover, the Fe₃O₄-Ag^{MBA}@Au NPs facilitated pre-purifying sample using magnetic separation, and complex matrix interference would be greatly decreased in the detection. The Fe₃O₄-Ag^{MBA}@Au NPs modified with N protein recognized and bound with N protein antibodies, which were trapped on the T-line, forming color band for observing detection. Under optimal conditions, the N protein antibodies could be qualitatively detected in colorimetric mode with the visual limit of 10⁻⁸ mg/mL and quantitatively detected by SERS signals between 10⁻⁶ and 10⁻¹⁰ mg /mL with 0.08 pg/mL detection limit. The coefficients variations (CV) of intra-assay was 8.0%, whereas of inter-assay was 11.7%, confirming of good reproducibility. Finally, this approach was able to discriminate between positive, negative, and weakly positive samples when detecting 107 clinical serum samples. The process enables highly sensitive quantitative assays that are valuable for evaluating disease processes and guiding treatment.

Keywords SARS-CoV-2 N protein antibody · Fe₃O₄-Ag^{MBA}@Au NPs · LFIA · SERS · Colorimetry

Introduction

Since December 2019, the severe acute respiratory syndrome coronavirus 2 (SARS-CoV-2) appeared and caused coronavirus disease 2019 (COVID-19), spreading globally at an alarming rate. The nucleic acid detection of

nasopharyngeal swabs is the gold standard to verify the infection of SARS-CoV-2 at present [1, 2]. However, the negative results obtained by this method need to be verified by several repeated detections because of its high false-negative rate. In addition to evaluating the viral nucleic acid, it has been demonstrated that detecting particular antibodies can help confirm SARS-CoV-2 infection, especially for individuals those with undetectable viral nucleic acid [3, 4].

When the virus infects human cells, the nucleocapsid (N) protein is highly expressed, which is essential for viral particle assembly. In the immunoassay for detecting SARS-CoV-2, the N protein is used as specific biomarker due to its high expression [5, 6]. Moreover, N protein is highly immunogenic; therefore, the human body produces

✉ Congying Wen
fleyxt@163.com

✉ Jingbin Zeng
xmuzjb@163.com

¹ College of Chemistry and Chemical Engineering, China University of Petroleum (East China), Qingdao 266580, People's Republic of China

many antibodies to it. And, an excellent association was seen between the amount of N protein antibodies in serum and the serum's ability to neutralize the virus [7]. Furthermore, N protein-specific antibodies do not necessarily indicate S-RBD neutralizing antibodies [7]. So N protein antibody testing is an essential sign for detecting the severity SARS-CoV-2 infection, which is helpful to guide clinical treatment [8–11]. Additionally, antibody testing can detect ongoing or past infections, thereby developing effective and accurate control strategies [12].

Currently, various analytical techniques have been developed based on different platforms, including enzyme-linked immunosorbent assay (ELISA) [13], microfluidic [14], chemiluminescence immunoassay (CLIA) [15, 16], and lateral flow immunoassay (LFIA) [17]. Among them, LFIA has received great attention with the distinctive virtues of being quick, simple, low-cost, portable, and friendly to users [18]. However, due to their limited sensitivity and difficulty in quantitative detection, traditional LFIAs based on gold nanoparticles may not meet present detection requirements. Besides, the single detection mode based on colorimetric results is susceptible to interference from biological environment with high background, particularly serum and plasma. Recent studies have applied colorimetric/fluorescence [19], colorimetric/luminescence [20] and colorimetric/surface-enhanced Raman spectroscopy (SERS) [21, 22] dual-mode analytical models to LFIA platform [4], based on colloidal gold [17], carbon nanoparticles [23], fluorescent nanoparticles [24–27], SERS-active nanomaterials [28, 29], and magnetic nanoparticles [30, 31] as the LFIA reporters.

One of these models is SERS, an ultrasensitive vibration spectroscopy technology, which has quick reaction time, excellent band resolution, and a wealth of fingerprint data. The nanotags used in SERS determine the accuracy and sensitivity of the readout signals [32, 33]. Gold and silver nanoparticles (Au and Ag NPs) are the main nanotags used for SERS-based detection of antibodies. However, they need to be combined with Raman reporter molecules to amplify the SERS signal [33, 34], which are easily disturbed by environmental interference. Typically, Au NPs are stable and biocompatible, while Ag NPs have much stronger SERS signal activity than Au NPs, yet they have a lower stability and poor surface functionalization [21, 35]. In the previous work, we used a ligand-assisted epaxial growth approach to encapsulate Ag NPs modified with 4-mercaptobenzoic acid (MBA) with an ultrathin gold shell for enhanced stability, bio-modification, and SERS performance [36]. Colorimetric and SERS modes were achieved to detect SARS-CoV-2 S protein antibody based on the $\text{Ag}^{\text{MBA}}\text{@Au}$ NPs. Although the detection was superior to the standard colloidal gold approach, the detection limit was larger than that of gold nanostars, and especially the detection limit in serum was

greater than that in PBS, suggesting interference by the complex matrix in serum.

In this study, we used magnetic nanoparticles as the core and coated a layer of $\text{Ag}^{\text{MBA}}\text{@Au}$ particles on the surface by electrostatic interaction to prepare $\text{Fe}_3\text{O}_4\text{-Ag}^{\text{MBA}}\text{@Au}$ probes with magnetic-Raman-colorimetric properties. Each Fe_3O_4 nanoparticle carries multiple $\text{Ag}^{\text{MBA}}\text{@Au}$ NPs, which can greatly enhance the magnitude of the SERS signal readout. Moreover, using magnetic properties of Fe_3O_4 to enrich and purify the targets from the samples can effectively avoid the interference from the matrix. Then, $\text{Fe}_3\text{O}_4\text{-Ag}^{\text{MBA}}\text{@Au}$ NPs conjugated with the SARS-COV-2 N protein were employed as the dual-signal colorimetric/SERS probes. Combined with LFIA platform, we developed an approach for quantification of SARS-COV-2 N protein antibodies in actual serum samples, which showed much higher sensitivity and great promise for direct use in more complicated samples such as plasma. Moreover, the $\text{Fe}_3\text{O}_4\text{-Ag}^{\text{MBA}}\text{@Au}$ NPs-based LFIA enable simple and rapid detection in epidemic areas, which has the potential to be popularized to the detection of other pathogens or antibodies.

Experimental section

Reagents and samples

AgNO_3 , NaBH_4 , Na_2SO_3 , NaOH , KH_2PO_4 , Na_2HPO_4 , NaCl , H_2O_2 , FeCl_3 , ethylene glycol, sodium acetate, and KCl were of AR grade and used without additional purification. Trisodium citrate (TSC), L-ascorbic acid (L-AA), and polyvinylpyrrolidone (PVP, MW = 10,000) were purchased from Macklin Biochemical Co., Ltd (Shanghai, China). N-hydroxysuccinimide (NHS), chloroauric acid (HAuCl_4), sucrose, MBA, and 1-(3-dimethylaminopropyl)-3-ethylcarbodiimide hydrochloride (EDC) were purchased from Energy Chemical Co., Ltd (Shanghai, China). $\text{HS-(PEG)}_n\text{-COOH}$ (MW = 2000) was purchased from ToYongBio Tech. Inc. (Shanghai, China). SARS-CoV-2 spike protein, mouse anti-N protein antibody, and rabbit anti-human IgG were purchased from Sino Biological Inc. (Beijing, China). Mouse anti-*Staphylococcus aureus* antibody and mouse anti-*Salmonella typhimurium* antibody were purchased from Sigma-Aldrich (Saint Louis, MO, USA). SARS-CoV-2 N protein antibody was purchased from Abcam. Bovine serum albumin (BSA) was purchased from Labgic Technology Co., Ltd. (Beijing, China). Tween-20 was purchased from EKEAR Bio@Tech Co., Ltd. (Shanghai, China). Glass fiber conjugate pad, nitrocellulose membrane (NC membrane), PVC substrate, and absorbent pad were purchased from Joey-biotech Co., Ltd. (Shanghai, China). Serum samples were taken from the affiliated hospital of Qingdao University and stored at $-20\text{ }^\circ\text{C}$ for use.

Instruments

A Millipore Autopure WR600A system was used to obtain ultrapure water with a purity level of 18.2 M Ω -cm. On a UV-2450 spectrophotometer (Shimadzu), Ultraviolet visible (UV-vis) absorption spectra were analyzed. The iPhone11 (Apple) was used to capture the photos. Transmission electron microscopy (TEM) pictures were collected by a JEM 1400 microscope (JEOL). The Tecnai F30 microscope (Philips, FEI, TECNAI) was used for energy-dispersive X-ray elemental mapping (EDX) and high-resolution TEM (HR-TEM) investigations. The Raman scattering spectra were measured on the SR-510PRO Raman analyzer (Ocean optics). The test strips were sprayed by HGS510 (AUTOKUN) and divided by HGS210 induction cutting machine (AUTOKUN).

Ag^{MBA}@Au NPs synthesis process

The Ag^{MBA}@Au NPs were synthesized utilizing the approach from the previous study [36]. Briefly, by combining the seed-mediated growth and thermal reduction of AgNO₃ with citrate in a step-wise growth procedure, the stable Ag NPs were obtained [37]. The Au shell encapsulation method used sulfites to epitaxially deposit Au onto the surface of Ag nanostructures, resulting in size-controlled Ag@Au nanospheres with excellent plasma properties and good stability, as well as endurance in SERS applications [38]. The procedure was described in extensive detail in the Supporting Information.

Preparation of Fe₃O₄ NPs

In a 100-mL flask, we mixed 80 mL of ethylene glycol with 2.6 g of anhydrous ferric chloride, 1.0 g of sodium citrate, and 4.0 g of sodium acetate. The solute was completely dissolved under vigorous stirring. Then, after 12 h of reaction at 200 °C, the product resulted from the mixed solution was cooled to room temperature in a 100-mL Teflon-lined reaction kettle. And, the product was washed three times in a magnetic field with ethanol and ultrapure water and vacuum-dried at 60 °C for 12 h.

Preparation of Fe₃O₄-Ag^{MBA}@Au NPs (MNPs)

Ag^{MBA}@Au NPs were assembled onto Fe₃O₄ surface by electrostatic interaction (Fig. 1a). Specifically, 0.1 g of Fe₃O₄ was dispersed in 10 mL of ultrapure water, followed by the addition of 50 mL hydrochloric acid (0.1 M), and the mixture ultrasonically oscillated for 10 min. The Fe₃O₄ NPs were washed three times with ultrapure water to remove excess hydrochloric acid and finally dispersed in 5 mL of ultrapure water. The above Fe₃O₄ was mixed with 45 mL of

1% PEI solution, after ultrasonic vibration for 1 h, washed three times in ultrapure water, and then redispersed in 10 mL of ultrapure water. 1 mL of the above PEI-modified Fe₃O₄ solution was mixed with a certain volume of Ag^{MBA}@Au solution and ultrasonically oscillated to assemble the Ag^{MBA}@Au on the Fe₃O₄ surface. The free Ag^{MBA}@Au NPs were washed away by magnetic separation, and the assembled product was dispersed in 10 mL of ultrapure water.

Functionalization of Fe₃O₄-Ag^{MBA}@Au NPs

After adding 10 mL of a solution containing Fe₃O₄-Ag^{MBA}@Au NPs to 5.0 mL of a solution containing HS-(PEG) n-COOH (5.0 mg/mL), then the mixture was shaken vigorously for an hour at room temperature. Fe₃O₄-Ag^{MBA}@Au NPs were performed three washes in PBS (10 mM, pH = 6.8) by magnetic separation and then dispersed. To the above solution, following the successive addition of 100 μ L of 10 mg/mL NHS and 100 μ L of 20 mg/mL EDC, the resulted solution was gently shaken for 30 min at room temperature. Then, the nanoparticles were magnetically separated and washed several times with PBS before being dispersed in 1 mL of PBS with 10 μ g of SARS-COV-2 N protein. The mixture was shaken vigorously for 2 h at room temperature. Subsequently, the BSA solution was added to the immunofunctionalized nanoparticles (IMNPs) and shaken on a shaker for 30 min. Finally, after washing with PBS, the obtained IMNPs were redispersed into a solution of 1% Tween-20, 1% BSA, 1% sucrose in PBS, and stored at 4 °C.

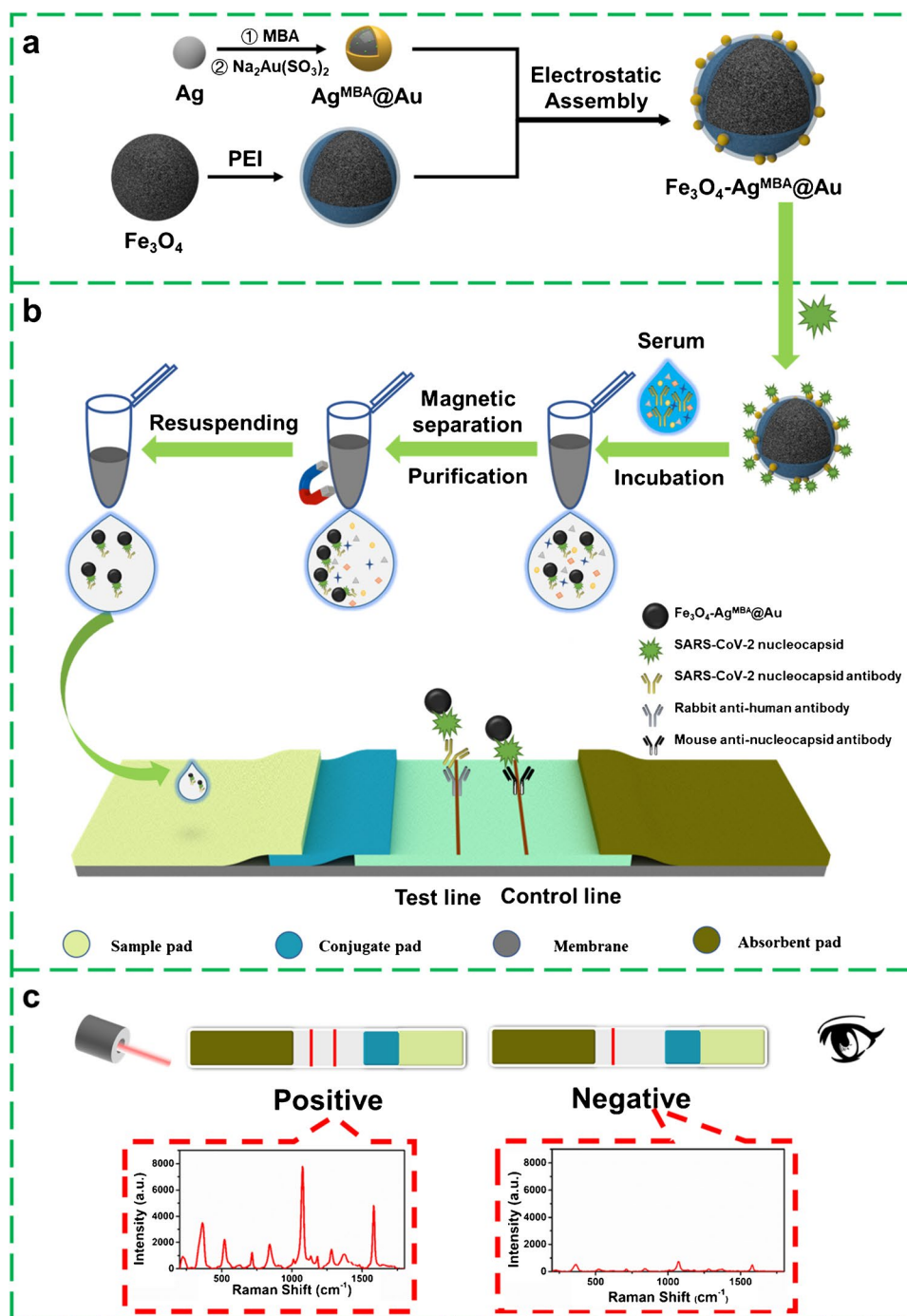
Fabrication of the LFIA strip

Wet-method LFIA is utilized to identify SARS-COV-2 N protein antibody, as illustrated in Fig. 1b. The test strip is organically assembled from five parts: nitrocellulose membrane, sample pad, binding pad, absorption pad, and PVC substrate. First, the sample pad, binding pad, absorbent pad, and nitrocellulose membrane were pasted on the PVC substrate in an overlapping manner, with an overlap of 2 mm. Then, at a rate of 1.0 μ L cm⁻¹, 1 mg/mL mouse anti-SARS-CoV-2 N protein antibody and 1 mg/mL rabbit anti-human antibody were sprayed onto the T-line and C-line, respectively. After 12 h of drying at 37 °C, the sprayed test strips were slit to a width of 3 mm and kept at 25 °C until further usage.

Detection of N protein antibody with the dual-mode LFIA in simulated serum

Serum from healthy volunteers was spiked with various amounts of SARS-CoV-2 N protein antibody to make simulated samples. Following a tenfold dilution in PBS,

Fig. 1 **a** Synthesis schematic of $\text{Fe}_3\text{O}_4\text{-Ag}^{\text{MBA}}\text{@Au}$ NPs. **b** Diagram of the detection principle and test strip for detecting human SARS-CoV-2 N protein antibody using $\text{Fe}_3\text{O}_4\text{-Ag}^{\text{MBA}}\text{@Au}$ NPs. **c** Interpretation of test results



the samples were analyzed with dual-mode LFIA. In a centrifuge tube, after thoroughly mixing 40 μL of the SARS-CoV-2 N protein antibody with a specified quantity of the IMNPs, the final volume was adjusted to 200 μL by adding 0.01 M PBS (pH = 7.4). The mixed solution was shaken at 150 rpm on a shaker, and then the IMNPs were collected using a magnetic separator. After being washed in 0.01 M PBS (pH = 7.4), the resulting precipitate was

dispersed in 100 μL of running solution (0.01 M pH = 7.4 PBS with 2% Tween-20 and 1.5% BSA) and then added to the microplate. The test strip's sample pad was inserted into the microplate's solution. After 20 min, the color of the T-line was visually observed for qualitative detection. And the intensity of Raman peak at 1075 cm^{-1} was measured using portable Raman spectrometer equipped with a 785 nm laser for quantitative detection.

Application to clinical samples

Blood samples from 9 unvaccinated and 98 vaccinated volunteers were stored overnight and centrifuged at $1000 \times g$ for 20 min at 4 °C and then detected. Before being analyzed with this abovementioned protocol, the samples were diluted tenfold with PBS.

Results and discussion

Dual-mode LFIA principle for detecting SARS-CoV-2 N protein antibody

The detection method is shown in Fig. 1b. The IMNPs are added to the serum samples to bind with N protein antibody via antigen–antibody interaction, and then magnetic separation is used to eliminate interference from other matrices (such as other antibodies in serum and proteins) in the serum sample. Following magnetic separation, the immune complexes were redispersed and transferred onto the test strip sample pad, which were caught by the rabbit anti-human antibodies on the T-line, resulting a colorful band. For quality control, the mouse anti-SARS-CoV-2 N protein antibody captured free nanomaterials onto the C-line. As shown in Fig. 1c, the visual-based colorimetric detection mode shows that two obvious dark-gray bands on the T- and C-lines for positive samples and only one band on the C-line for negative samples, while the others were invalid. A portable Raman spectrometer could be used to measure the SERS signal for quantitative detection. The dual-signal readout of $\text{Fe}_3\text{O}_4\text{-Ag}^{\text{MBA}}\text{@Au}$ NPs made it possible to do both qualitative and quantitative analyses using naked eyes and instrument, respectively.

Characterization of $\text{Fe}_3\text{O}_4\text{-Ag}^{\text{MBA}}\text{@Au}$ composite nanoparticles

The composite nanoparticles used in this study were created by electrostatically assembling $\text{Ag}^{\text{MBA}}\text{@Au}$ NPs onto the surface of Fe_3O_4 . This approach effectively preserved the nanoparticles' basic morphology, Raman optical properties, and magnetic properties. The oxidation state of element Fe in the synthesized nanoparticles was confirmed by XPS (Fig. S1), which in turn confirmed the successful synthesis of Fe_3O_4 NPs. On this basis, we performed other characterizations of Fe_3O_4 NPs and the composite particles. The TEM images showed that the synthesized $\text{Ag}^{\text{MBA}}\text{@Au}$ and Fe_3O_4 NPs were in good dispersity and uniform size with sphere appearance (Fig. 2a–b). The average particle sizes of $\text{Ag}^{\text{MBA}}\text{@Au}$ and Fe_3O_4 NPs were 32 ± 1 nm and 165 ± 6 nm, respectively, indicating that $\text{Ag}^{\text{MBA}}\text{@Au}$ and Fe_3O_4 NPs had good homogeneity. After the assembly is completed,

$\text{Ag}^{\text{MBA}}\text{@Au}$ NPs aggregated around Fe_3O_4 particles (Fig. 2c). As shown in Fig. 2d, about dozens of $\text{Ag}^{\text{MBA}}\text{@Au}$ particles were clustered around one Fe_3O_4 particle, which would enhance SERS signal intensity of the composite nanoparticles. The EDX images shown in Fig. 2e–i revealed that the outer periphery of the prepared composite nanoparticles was composed of $\text{Ag}^{\text{MBA}}\text{@Au}$ NPs, whereas the inner was composed of Fe_3O_4 NPs. And by examining the UV–vis spectra of MNPs and Fe_3O_4 alone, it can be seen from Fig. 2j that Fe_3O_4 alone has no obvious absorption peak between 300 and 900 nm, while MNPs has a characteristic peak at 422 nm. This characteristic peak is slightly red-shifted compared to $\text{Ag}^{\text{MBA}}\text{@Au}$ alone (408 nm). This may be caused by the aggregation of $\text{Ag}^{\text{MBA}}\text{@Au}$ nanoparticles. And Fig. 2k shows the magnetic behavior of Fe_3O_4 NPs and $\text{Fe}_3\text{O}_4\text{-Ag}^{\text{MBA}}\text{@Au}$ NPs. The saturation magnetization (Ms) of Fe_3O_4 NPs and $\text{Fe}_3\text{O}_4\text{-Ag}^{\text{MBA}}\text{@Au}$ NPs were found to be 30.3 emu/g and 26.6 emu/g, respectively. Thus, the Ms of Fe_3O_4 NPs was decreased by the absorption of the $\text{Ag}^{\text{MBA}}\text{@Au}$ NPs on their surface. The above characterization confirmed that $\text{Fe}_3\text{O}_4\text{-Ag}^{\text{MBA}}\text{@Au}$ NPs were successfully synthesized.

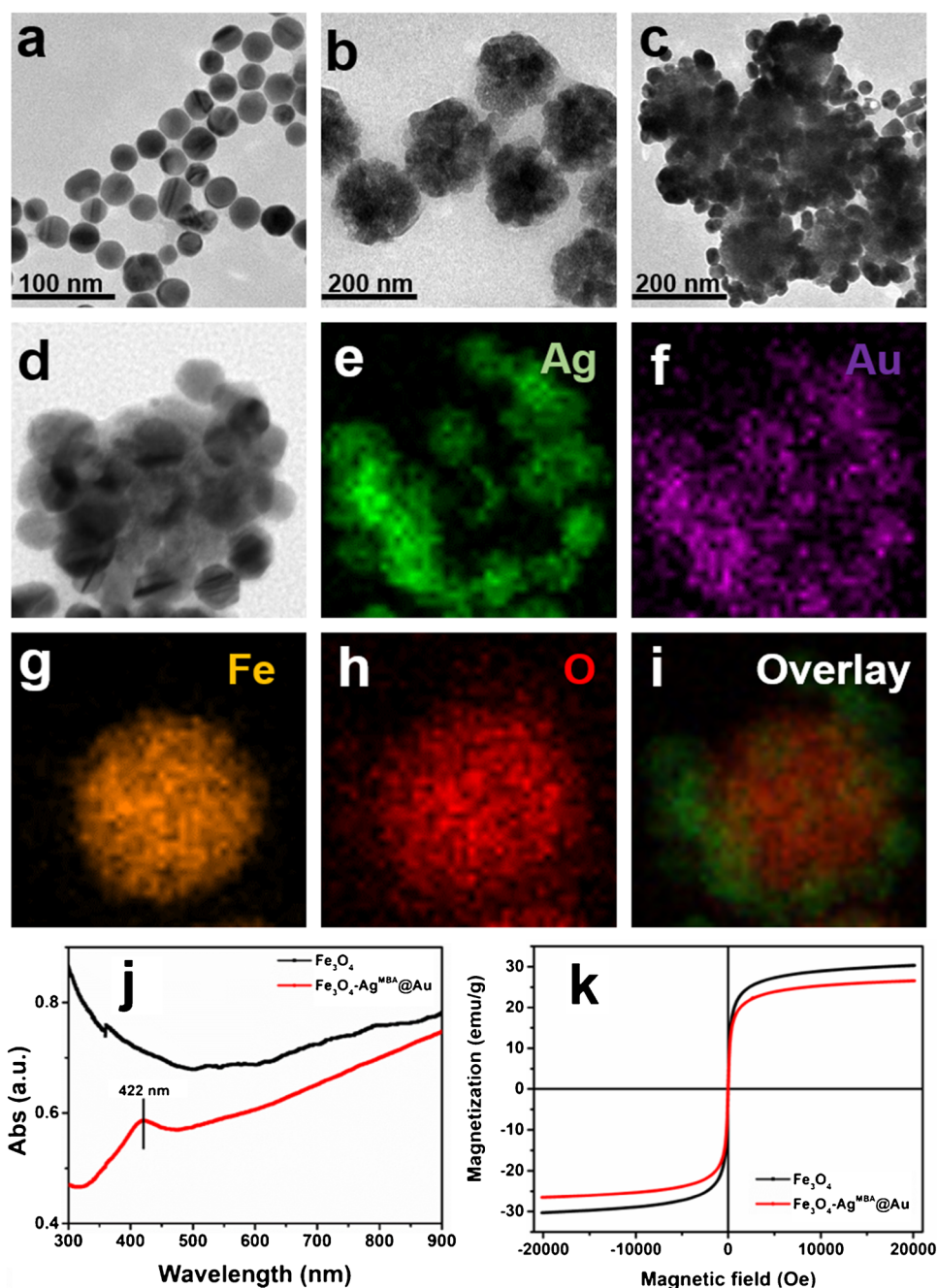
Next, we optimized the assembling conditions. With the increasing volume of $\text{Ag}^{\text{MBA}}\text{@Au}$ nanoparticles assembled and the binding time, the SERS signal of $\text{Fe}_3\text{O}_4\text{-Ag}^{\text{MBA}}\text{@Au}$ NPs increased continuously (Fig. 3a–b). When 30 mL $\text{Ag}^{\text{MBA}}\text{@Au}$ was added to 1 mg Fe_3O_4 , the SERS signal reached the highest, presumably because the surface sites of Fe_3O_4 were virtually entirely occupied by $\text{Ag}^{\text{MBA}}\text{@Au}$ particles. When the binding time reached 40 min, the SERS signal reached its maximum value, which was very close to the value observed after 30 min of binding. We finally selected 30 min as the optimal binding time. As shown in Fig. 3c, we verified the relationship between the concentration of $\text{Fe}_3\text{O}_4\text{-Ag}^{\text{MBA}}\text{@Au}$ NPs and the intensity of Raman spectra and found that there was a good linear relationship ($R^2 = 0.999$), which enabled quantitative detection based on the SERS signal.

Dual-mode LFIA performance in the detection of SARS-CoV-2 N protein antibody in serum

To obtain the ideal conditions for detection, we optimized the concentration of BSA in the blocking solution, the amount of IMNPs, and the amount of conjugated antibody on IMNPs (Fig. S2a–c). Finally, we chose 15% BSA, 30 μL of the probe solution, and 15 μg of conjugated antibody as the ideal conditions.

Under the optimized conditions, we evaluated the method's sensitivity and linear range for detecting SARS-CoV-2 N protein antibody with concentration gradient of 0, 10^{-10} , 10^{-9} , 10^{-8} , 10^{-7} , and 10^{-6} mg/mL. As shown in Fig. 4a, for samples without target antibodies, just the C line

Fig. 2 Characterizing $\text{Fe}_3\text{O}_4\text{-Ag}^{\text{MBA}}\text{@Au}$ NPs. **a–c** TEM images of $\text{Ag}^{\text{MBA}}\text{@Au}$, Fe_3O_4 , and MNPs. **d** High-resolution TEM image of a single MNP. **e–i** EDX elemental analyses of Ag, Au, Fe, O, and their overlay. **j** UV–vis spectra of Fe_3O_4 and MNPs. **k** Hysteresis loops of Fe_3O_4 and MNPs



of the test strip displayed color. Once the antibody concentration reached 10^{-8} mg/mL or more, the T-line is visible to the naked eyes as a dark-gray band, and its color gradually deepened as the antibody concentration rose. In addition, we compared the effect of magnetic separation on the detection signal. SERS signals were found to be stronger in samples with magnetic separation enrichment, as indicated in Fig. 4b, implying that the enrichment step greatly reduced the matrix interference in the samples, thereby improving the sensitivity. For accurate quantitative analysis, portable Raman spectrometer was used to collect the T-line SERS spectra. As

shown in Fig. 4c and d, the relationship between the target antibody concentration and the intensity of the maximum scattering peak at 1075 cm^{-1} was excellently linear within the range of 10^{-10} to 10^{-6} mg/mL ($R^2=0.995$). SERS analysis has the detection limit three orders of magnitude lower than visual detection, calculated to be 0.08 pg/mL from the minimal detectable signal (the average signal intensity plus triple standard deviation of the blank sample, $n=12$). In addition, the detection sensitivity is approximately six times more than that of S protein antibody detection by $\text{Ag}^{\text{MBA}}\text{@Au}$ NPs alone. Moreover, comparing various LFIA reporters

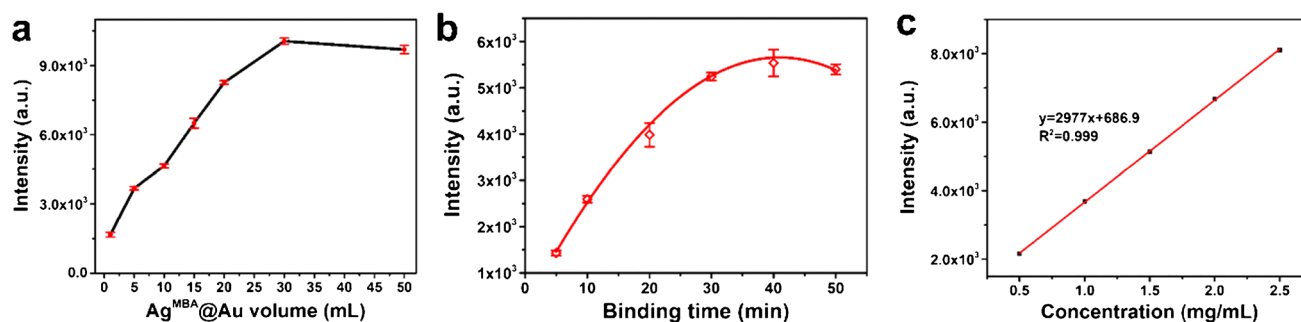
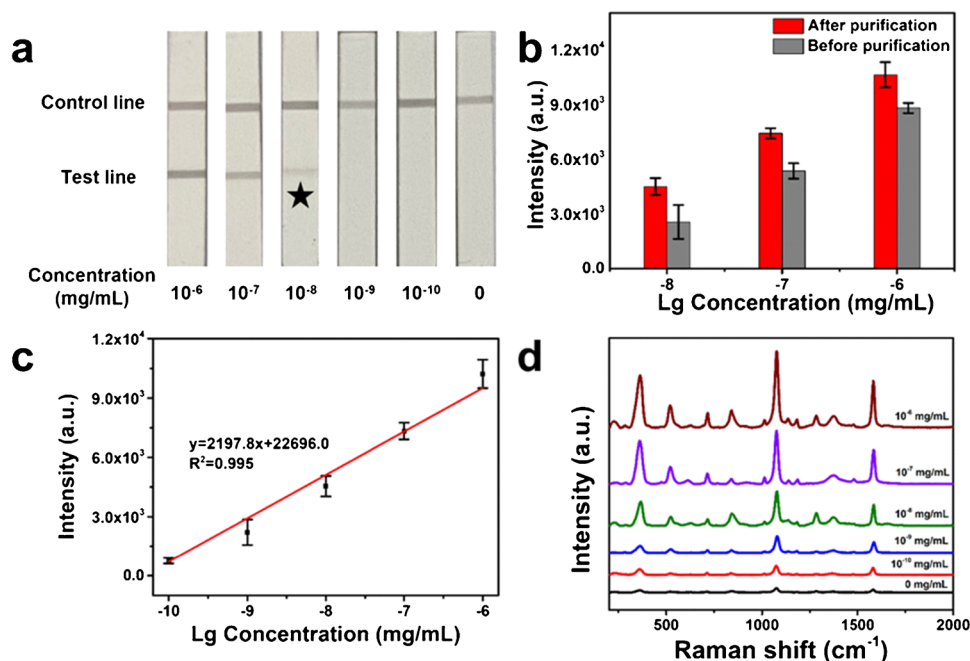


Fig. 3 **a** Optimization of the dosage of Ag^{MBA}@Au nanoparticles. **b** Optimization of binding time. **c** Linear relationship between particle concentration and Raman intensity

Fig. 4 **a** Photographs of SARS-CoV-2 N protein antibody detection test strips (visible detection limit is 10⁻⁸ mg/mL).

b The influence of magnetic separation on detection results. **c** Linear regression between the intensity of SERS signal at 1075 cm⁻¹ and SARS-CoV-2 N protein antibody concentration ranging from 10⁻¹⁰ to 10⁻⁶ mg/mL. Error bars are computed using data from three independent experiments. **d** Corresponding Raman spectra of the test strips with various concentrations of SARS-CoV-2 N protein antibodies in serum



for detecting SARS-CoV-2 N protein antibodies [19, 34, 39–42], SERS-based LFIA demonstrated significantly lower detection limit and wider linear range. In particular, our assay is three orders more sensitive than one using Au gap-enhanced Raman nanotags (GERTs) [34]. This method's excellent performance was owing to the incorporation of magnetic Fe₃O₄ particles, which could boost the SERS signal by aggregating Ag^{MBA}@Au particles and minimize the interference of complex substrates by magnetic separation.

Specificity and reproducibility

The specificity and reproducibility of the dual-mode immunoassay were studied further. To examine the specificity of this method, several proteins were added to serum samples for detecting the related SERS intensity, including SARS-CoV-2 N protein, SARS-CoV-2 N protein antibody,

SARS-CoV-2 S protein antibody, SARS-CoV-2 neutralizing antibody, anti-*Staphylococcus aureus* antibody and anti-*Salmonella typhimurium* antibody. As shown in Fig. 5, only 0.01 µg/mL, the target antibody could generate an obvious signal on the T-line, while even if the concentration of other samples was 100 to 200 times higher, they did not create any discernible differences compared to the negative samples. Therefore, this approach had satisfactory specificity and enabled the accurate detection of the target N protein antibody in complex matrix. To further study the test strips' reproducibility, we calculated the intra-assay and inter-assay coefficient of variation (CV) values in serum. As displayed in Table 1, the mean CV values were 8.0% for intra-assay and 11.7% for inter-assay, indicating good reproducibility for our method. Overall, the above results manifested that our dual-model immunoassay had high accuracy and reliability.

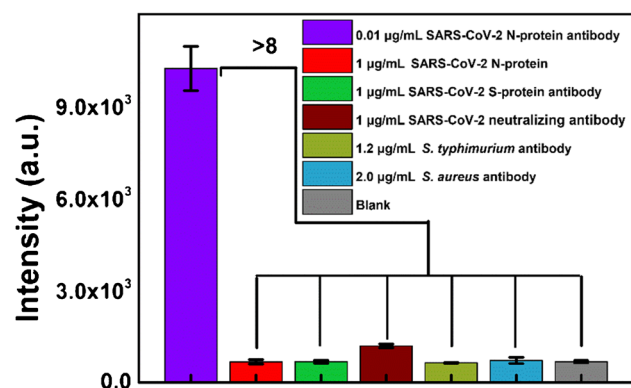


Fig. 5 Specificity of the dual-mode LFIA method by adding various antibodies and proteins to serum

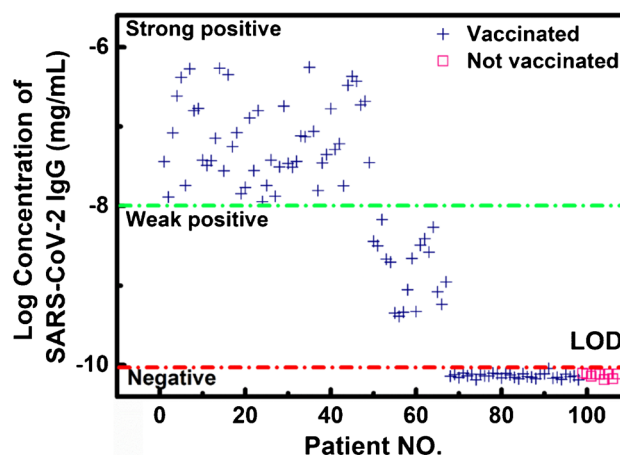


Fig. 6 Actual sample testing results based on the dual-mode LFIA

Detection of actual samples

To investigate the feasibility of this method in practical application, we collected serum samples from 107 volunteers, including 9 unvaccinated and 98 vaccinated volunteers. The results were displayed in Fig. 6 and Table S2. Results with T-line visible was considered strong positive. Results whose T-line was not visible but could be identified with a portable Raman equipment was considered weak positive. Negative results were below Raman's detection limit. Of the vaccinated samples, 49 were strong positive, 18 were weakly positive, and the rest were all negative, while the 9 unvaccinated samples were all negative. Antibodies should be present in the vaccinated samples, but there is a wide range in antibody production following vaccination due to factors such as the timing of vaccination (no antibodies can usually be detected immediately following vaccination, and antibody levels in vaccinated volunteers are decreasing over time) and individual variation in immunity. The results demonstrated that our approach could properly identify antibody levels in serum for outbreak control and vaccine guidance.

Conclusions

In conclusion, a new type of nanoprobe was created by combining the Fe_3O_4 NPs and $\text{Ag}^{\text{MBA}}@Au$ NPs, based on which, a dual-mode colorimetric/SERS LFIA platform was

successfully constructed for detecting oSARS-CoV-2 N protein antibody in an ultrasensitive mode. $\text{Ag}^{\text{MBA}}@Au$ NPs with Ag cores and ultra-thin Au shells displayed exceptional SERS properties, as well as good stability and biocompatibility. The magnetic nanoparticle Fe_3O_4 could boost the SERS signal intensity due to emble numerous $\text{Ag}^{\text{MBA}}@Au$ NPs assembled on its surface, while its magnetic characteristic could also be employed to remove complicated substrates, thus highly improving detection sensitivity and anti-interference ability. Taking advantages of the superior dual signal readout of colorimetric/SERS, the designed LFIA for detecting SARS-CoV-2 N protein antibody had visual detection limit of 10^{-8} mg/mL, and the quantitative detection limit reached 0.08 pg/mL by SERS, three orders of magnitude more sensitive than visual detection. In addition, our assay substantially improved the sensitivity of detecting SARS-COV-2 N protein antibody compared to other LFIA reporters. Besides, the developed detection platform demonstrated rapidity, efficiency, and accuracy in serum samples. Moreover, we successfully used it to identify the target antibody levels in actual samples. While the proposed platform was successful in detecting total antibodies, it cannot discriminate subclasses like IgM, IgE, and IgG, which provide more information on the progression of an infection or the efficacy of vaccine. So, making multi-channel strips for the combined quantitative detection of IgG and IgM can make the test more accurate and confirm the course of an infection better.

Table 1 Dual-mode LFIA reproducibility test based on $\text{Fe}_3\text{O}_4\text{-Ag}^{\text{MBA}}@Au$ NPs in serum

Antibody concentration (mg/mL)	Intra-assay			Inter-assay		
	Mean	SD	CV (%)	Mean	SD	CV (%)
10^{-6}	10,227	720	7.0	11,583	1164	14.1
10^{-7}	7335	421	5.7	7510	455	6.1
10^{-8}	4543	519	11.4	4416	625	14.5
Intra-assay variability				Inter-assay variability		
8.0%				11.7%		

Consequently, the dual-mode and multi-channel LFIA platform has significant potential for in situ and real-time detection, which is crucial for nations or regions with limited resources.

Supplementary Information The online version contains supplementary material available at <https://doi.org/10.1007/s00216-022-04437-1>.

Author contribution Conceptualization: J.B. Zeng, J.W. Li. Validation: J.W. Li, P.H. Liang. Methodology: J.B. Zeng, J.W. Li. Analysis: P.H. Liang, T.Y. Zhao, G.C. Guo, J.Y. Zhu. Writing—original draft: J.W. Li, P.H. Liang. Writing—review and editing: J.B. Zeng, C.Y. Wen. Supervision: J.B. Zeng, C.Y. Wen. Project administration: J.B. Zeng. All authors have read and agreed to the published version of the manuscript.

Funding This work was supported by the Key Fundamental Project of Shandong Natural Science Foundation (Z.J., ZR2020ZD13), the Natural Science Foundation of Shandong (W.C., ZR2020MB064), the Fundamental Research Funds for the Central Universities (L.J., 21CX06014A; W.C., 22CX03033A), the Science and Technology Projects of Qingdao (Z.J., 21-1-4-sf-7-nsh), and the National Natural Science Foundation of China (Z.J., no. 21876206).

Declarations

Ethics approval All included volunteers gave their oral and informed consent. The study was approved by the Medical Ethics Committee of the Affiliated Hospital of Qingdao University (number: QYFYKYL 984311920).

Source of biological material The serum samples from 107 volunteers, including 9 unvaccinated and 98 vaccinated volunteers, were collected from the Affiliated Hospital of Qingdao University.

Competing interest The authors declare no competing interests.

References

- Pan Y, Zhang D, Yang P, Poon LLM, Wang Q. Viral load of SARS-CoV-2 in clinical samples. *Lancet Infect Dis*. 2020;20(4):411–2.
- Wang W, Xu Y, Gao R, Lu R, Han K, Wu G, et al. Detection of SARS-CoV-2 in different types of clinical specimens. *Jama-J Am Med Assoc*. 2020;323(18):1843–4.
- Dong X, Cao Y-Y, Lu X-X, Zhang J-J, Du H, Yan Y-Q, et al. Eleven faces of coronavirus disease 2019. *Allergy*. 2020;75(7):1699–709.
- Guo JC, Chen SQ, Guo JH, Ma X. Nanomaterial labels in lateral flow immunoassays for point-of-care-testing. *J Mater Sci Technol*. 2021;60:90–104.
- Kang S, Yang M, Hong Z, Zhang L, Huang Z, Chen X, et al. Crystal structure of SARS-CoV-2 nucleocapsid protein RNA binding domain reveals potential unique drug targeting sites. *Acta Pharm Sin B*. 2020;12:1228–38.
- Perdikari TM, Murthy AC, Ryan VH, Watters S, Naik MT, Fawzi NL. SARS-CoV-2 nucleocapsid protein phase-separates with RNA and with human hnRNPs. *Embo J*. 2020;39(24):106478.
- McAndrews KM, Dowlatshahi DP, Dai J, Becker LM, Hensel J, Snowden LM, et al. Heterogeneous antibodies against SARS-CoV-2 spike receptor binding domain and nucleocapsid with implications for COVID-19 immunity. *Jci Insight*. 2020;5(18):142386.
- Kiew LV, Chang CY, Huang SY, Wang PW, Heh CH, Liu CT, et al. Development of flexible electrochemical impedance spectroscopy-based biosensing platform for rapid screening of SARS-CoV-2 inhibitors. *Biosens Bioelectron*. 2021;183:113213.
- Huang LR, Chiu CM, Yeh SH, Huang WH, Hsueh PR, Yang WZ, et al. Evaluation of antibody responses against SARS coronavirus nucleocapsid or spike proteins by immunoblotting or ELISA. *J Med Virol*. 2004;73(3):338–46.
- Shang B, Wang XY, Yuan JW, Vabret A, Wu XD, Yang RF, et al. Characterization and application of monoclonal antibodies against N protein of SARS-coronavirus. *Biochem Biophys Res Commun*. 2005;336(1):110–7.
- Wang J, Ji J, Ye J, Zhao X, Wen J, Li W, et al. The structure analysis and antigenicity study of the N protein of SARS-CoV. *Genom Proteom Bioinf*. 2003;1(2):145–54.
- Li H, Pan J, Su Y, Wang B, Ge J. SARS-CoV-2 IgM/IgG antibody detection confirms the infection after three negative nucleic acid detection. *J Cell Mol Med*. 2020;24(14):8262–5.
- Larsen SE, Berube BJ, Pecor T, Cross E, Brown BP, Williams BD, et al. Qualification of ELISA and neutralization methodologies to measure SARS-CoV-2 humoral immunity using human clinical samples. *J Immunol Methods*. 2021;499:113160.
- Ng AHC, Fobel R, Fobel C, Lamanna J, Rackus DG, Summers A, et al. A digital microfluidic system for serological immunoassays in remote settings. *Sci Transl Med*. 2018;10:e6076.
- Lijia S, Lihong S, Huabin W. Serological chemiluminescence immunoassay for the diagnosis of SARS-CoV-2 infection. *J Clin Lab Anal*. 2020;34(10):e23466.
- Gambino CM, Lo Sasso B, Colomba C, Giglio RV, Agnello L, Bivona G, et al. Comparison of a rapid immunochromatographic test with a chemiluminescence immunoassay for detection of anti-SARS-CoV-2 IgM and IgG. *Biochimica medica*. 2020;30(3):030901.
- Huang C, Wen T, Shi FJ, Zeng XY, Jiao YJ. Rapid detection of IgM antibodies against the SARS-CoV-2 virus via colloidal gold nanoparticle-based lateral-flow assay. *ACS Omega*. 2020;5(21):12550–6.
- Bahadir EB, Sezginurk MK. Lateral flow assays: principles, designs and labels. *Trac-Trends Anal Chem*. 2016;82:286–306.
- Chen Z, Zhang Z, Zhai X, Li Y, Lin L, Zhao H, et al. Rapid and sensitive detection of anti-SARS-CoV-2 IgG, using lanthanide-doped nanoparticles-based lateral flow immunoassay. *Anal Chem*. 2020;92(10):7226–31.
- Liu D, Ju C, Han C, Shi R, Chen X, Duan D, et al. Nanozyme chemiluminescence paper test for rapid and sensitive detection of SARS-CoV-2 antigen. *Biosens Bioelectron*. 2021;173:112817.
- Liu H, Dai E, Xiao R, Zhou Z, Zhang M, Bai Z, et al. Development of a SERS-based lateral flow immunoassay for rapid and ultra-sensitive detection of anti-SARS-CoV-2 IgM/IgG in clinical samples. *Sens Actuators B Chem*. 2021;329:129196.
- Srivastav S, Dankov A, Adanalic M, Grzeschik R, Vi T, Pagel-Wieder S, et al. Rapid and sensitive SERS-based lateral flow test for SARS-CoV2-specific IgM/IgG antibodies. *Anal Chem*. 2021;93(36):12391–9.
- Zhang X, Yu X, Wen K, Li C, Mujtaba Mari G, Jiang H, et al. Multiplex Lateral Flow Immunoassays Based on Amorphous Carbon Nanoparticles for Detecting Three *Fusarium* Mycotoxins in Maize. *J Agric Food Chem*. 2017;65(36):8063–71.
- Taranova NA, Berlina AN, Zherdev AV, Dzantiev BB. ‘Traffic light’ immunochromatographic test based on multicolor quantum dots for the simultaneous detection of several antibiotics in milk. *Biosens Bioelectron*. 2015;63:255–61.
- Beloglazova NV, Sobolev AM, Tessier MD, Hens Z, Goryacheva IY, De Saeger S. Fluorescently labelled multiplex lateral flow immunoassay based on cadmium-free quantum dots. *Methods*. 2017;116:141–8.

26. Huang C, Wei Q, Hu Q, Wen T, Xue L, Li S, et al. Rapid detection of severe fever with thrombocytopenia syndrome virus (SFTSV) total antibodies by up-converting phosphor technology-based lateral-flow assay. *Luminescence*. 2019;34(2):162–7.
27. Martiskainen I, Talha SM, Vuorenmaa K, Salminen T, Juntunen E, Chattopadhyay S, et al. Upconverting nanoparticle reporter-based highly sensitive rapid lateral flow immunoassay for hepatitis B virus surface antigen. *Anal Bioanal Chem*. 2021;413(4):967–78.
28. Fu X, Wen J, Li J, Lin H, Liu Y, Zhuang X, et al. Highly sensitive detection of prostate cancer specific PCA3 mimic DNA using SERS-based competitive lateral flow assay. *Nanoscale*. 2019;11(33):15530–6.
29. Su L, Hu H, Tian Y, Jia C, Wang L, Zhang H, et al. Highly sensitive colorimetric/surface-enhanced raman spectroscopy immunoassay relying on a metallic core-shell Au/Au nanostar with clenbuterol as a target analyte. *Anal Chem*. 2021;93(23):8362–9.
30. Cai Y, Yan J, Zhu L, Wang H, Lu Y. A rapid immunochromatographic method based on a secondary antibody-labelled magnetic nanoprobe for the detection of hepatitis B preS2 surface antigen. *Biosensors-Basel*. 2020;10(11):161–77.
31. Razo SC, Panferov VG, Safenkova IV, Varitsev YA, Zherdev AV, Dzantiev BB. Double-enhanced lateral flow immunoassay for potato virus X based on a combination of magnetic and gold nanoparticles. *Anal Chim Acta*. 2018;1007:50–60.
32. Xiao R, Lu L, Rong Z, Wang C, Peng Y, Wang F, et al. Portable and multiplexed lateral flow immunoassay reader based on SERS for highly sensitive point-of-care testing. *Biosens Bioelectron*. 2020;168:112524.
33. Wang Z, Zong S, Wu L, Zhu D, Cui Y. SERS-activated platforms for immunoassay: probes, encoding methods, and applications. *Chem Rev*. 2017;117(12):7910–63.
34. Chen S, Meng L, Wang L, Huang X, Ali S, Chen X, et al. SERS-based lateral flow immunoassay for sensitive and simultaneous detection of anti-SARS-CoV-2 IgM and IgG antibodies by using gap-enhanced Raman nanotags. *Sens Actuators B Chem*. 2021;348:130706.
35. Rycenga M, Xia X, Moran CH, Zhou F, Qin D, Li Z-Y, et al. Generation of hot spots with silver nanocubes for single-molecule detection by surface-enhanced raman scattering. *Angew Chem Int Ed*. 2011;50(24):5473–7.
36. Liang P, Guo Q, Zhao T, Wen C-Y, Tian Z, Shang Y, et al. Ag nanoparticles with ultrathin Au shell-based lateral flow immunoassay for colorimetric and SERS dual-mode detection of SARS-CoV-2 IgG. *Anal Chem*. 2022;94(23):8466–73.
37. Wan Y, Guo Z, Jiang X, Fang K, Lu X, Zhang Y, et al. Quasi-spherical silver nanoparticles: aqueous synthesis and size control by the seed-mediated Lee-Meisel method. *J Colloid Interface Sci*. 2013;394:263–8.
38. Liu H, Liu T, Zhang L, Han L, Gao C, Yin Y. Etching-free epitaxial growth of gold on silver nanostructures for high chemical stability and plasmonic activity. *Adv Funct Mater*. 2015;25(34):5435–43.
39. Wang Z, Zheng Z, Hu H, Zhou Q, Liu W, Li X, et al. A point-of-care selenium nanoparticle-based test for the combined detection of anti-SARS-CoV-2 IgM and IgG in human serum and blood. *Lab Chip*. 2020;20(22):4255–61.
40. Ahmadi A, Mirzaeizadeh Z, Omidfar K. Simultaneous detection of SARS-CoV-2 IgG/IgM antibodies, using gold nanoparticles-based lateral flow immunoassay. *Monoclon Antibodies Immunodiag Immunother*. 2021;40(5):210–8.
41. Chen C, Hu H, Li X, Zheng Z, Wang Z, Wang X, et al. Rapid DETECTION OF Anti-SARS-CoV-2 antibody using a selenium nanoparticle-based lateral flow immunoassay. *IEEE Trans Nanobiosci*. 2022;21(1):37–43.
42. Bayin Q, Huang L, Ren C, Fu Y, Ma X, Guo J. Anti-SARS-CoV-2 IgG and IgM detection with a GMR based LFIA system. *Talanta*. 2021;227:122207.

Publisher's note Springer Nature remains neutral with regard to jurisdictional claims in published maps and institutional affiliations.

Springer Nature or its licensor (e.g. a society or other partner) holds exclusive rights to this article under a publishing agreement with the author(s) or other rightsholder(s); author self-archiving of the accepted manuscript version of this article is solely governed by the terms of such publishing agreement and applicable law.